SMILES Summer School on Machine Learning: Identification of tumor-associated macrophages in diffuse large B-cell lymphoma using computer vision and Artificial Intelligence

Anastasiia Studenikina[1], Danil Sulimov[2], Dmitry Zvezdin[3], Arsenii Galimov[4], Olga Filimonova[3], Alibek Epkhiev[2], Ekaterina Anpilogova[5]
Project curator: Svetlana Illarionova [6]
[1] Moscow Institute of Physics and Technology, Moscow, Russia
[2] National Research University Higher School of Economics, Moscow, Russia
[3] Lomonosov Moscow State University, Moscow, Russia
[4] Institute of Plant and Animal Ecology UB RAS, Ekaterinburg, Russia
[5] Saint Petersburg State University, Saint Petersburg, Russia
[6] Skolkovo Institute of Science and Technology, Moscow, Russia

Abstract

The first approach based on self-supervised learning (SSL) with parameter-efficient fine-tuning is proposed for automated identification of tumor-associated macrophages (TAMs) on standard sections stained with hematoxylin and eosin (H&E) in diffuse large cell B-cell lymphoma (DLBCL). The approach utilized ResNet-18 architecture with SimCLR-based contrastive learning using NT-Xent loss function (Normalized Temperature-scaled Cross Entropy), enhanced by Low-Rank Adaptation (LoRA) for efficient parameter optimization. Based on 23 WSI microphotographs of DLBCL (856 manually annotated TAMs) supplemented with LyNSeC and Immunocto sets, the NT-Xent loss function ResNet-18 achieved an accuracy, exceeding the performance of traditional transfer learning. The proposed system successfully distinguishes TAM on H&E slices, eliminating the need for immunohistochemical (IHC) staining. However, despite the promising results, larger clinical trials are needed to confirm the prognostic significance.

Index Terms: Diffuse large B-cell lymphoma (DLBCL), Tumor-associated macrophages (TAM), Self-supervised learning (SSL), Contrastive learning, H&E staining, Digital pathology, Computer vision

1 Introduction

Diffuse large B-cell lymphoma (DLBCL) is an aggressive hematological malignancy, with approximately 150000 new cases diagnosed annually [14]. The overall five-year survival rate does not exceed 65%, and around 30–40% of patients remain resistant to standard immunotherapy [15]. Tumor-associated macrophages (TAMs) play a critical role in the tumor microenvironment and significantly impact disease prognosis [1, 18]. High TAM density has been associated with poor overall survival and more advanced DLBCL stages [11, 21], making the quantitative assessment of TAMs a clinically important task. Traditional methods for identifying TAMs rely on immunohistochemical (IHC) staining using specific antibodies such as CD68 and CD163 [8]. These methods require additional time, financial resources, and specialized equipment. Meanwhile, standard hematoxylin and eosin (H&E) staining does not allow easy identification of TAMs.

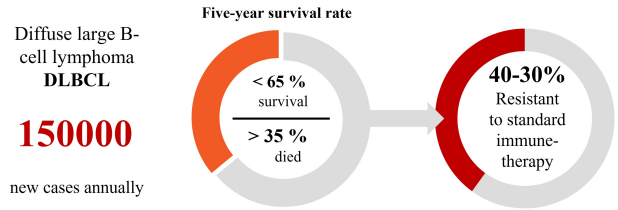

Figure 1. Incidence of DLBCL

1.1 Hypotheses

We propose the following hypotheses:

- ***H1:*** A ResNet-18 model pre-trained via self-supervised learning with contrastive NT-Xent loss (Normalized Temperature-scaled Cross Entropy) on unlabeled H&E-stained DLBCL histological images will demonstrate superior performance in tumor-associated macrophage (TAM) identification compared to models initialized with ImageNet weights or trained from scratch, due to domain-specific feature representations adapted to lymphoid tissue morphology
- ***H2:*** Integration of Low-Rank Adaptation (LoRA) with self-supervised pre-training will enable efficient fine-tuning for TAM classification while maintaining comparable or superior performance to full parameter fine-tuning, demonstrating parameter efficiency without sacrificing diagnostic accuracy.
- ***H3:*** The proposed SSL-based approach can effectively distinguish TAM from morphologically similar cell types (histiocytes, endothelial cells, reactive lymphoid elements) on standard H&E-stained sections without requiring IHC markers, achieving diagnostic performance comparable to expert pathologists.

1.2 Goals

To validate these hypotheses, we define actionable goals:

- **G1:** Develop and optimize a self-supervised learning framework based on SimCLR with NT-Xent contrastive loss specifically adapted for H&E-stained DLBCL histological images, incorporating LoRA for parameter-efficient adaptation and establishing superior feature representations compared to ImageNet pre-training baselines.
- **G2:** Create and validate an automated TAM identification system that achieves clinically relevant performance metrics on standard H&E-stained DLBCL tissue sections, demonstrating non-

Table 1
Models for histological image analysis

Model	Application	Features	Link
DeepCell	cell segmentation	H&E-stained histological images, not for TAM	Van Valen D. 2016 [17]
HoVer-Net	cell segmentation	H&E-stained histological images, not for TAM	Graham S. 2019 [4]
ConCORDe-Net	cell segmentation	IHC-stained histological images	Hagos Y. 2019. [5]
GOTDP-MP-CNNs	diagnosis of DLBCL	H&E-stained histological images, not for TAM	Li D. 2020 [7]
CellProfiler	cell segmentation	H&E-stained histological images, not for TAM	Stirling D. 2021 [16]
U-Net	cell segmentation	H&E-stained histological images, not for TAM	Manju P. 2023 [12]
HoLy-Net	DLBCL image segmentation	H&E-stained histological images, not for TAM	Naji H. 2024 [13]
Pathomics	predict DLBCL outcomes	H&E-stained histological images, not for TAM	Li Z. 2025 [10]

inferiority to expert pathologist assessment and eliminating the need for additional IHC staining.

2 Related work

Deep learning methods have shown impressive results in the histopathological diagnosis of DLBCL. Li et al. developed an ensemble platform comprising 17 convolutional neural networks (GOTDP-MP-CNNs), achieving 99 % accuracy in classifying DLBCL based on H&E-stained histological images—surpassing both conventional CNNs (87–96 %) and experienced pathologists (74 %) [7]. In 2020, an integrative model called "Pathomics" was introduced, combining clinical data with hundreds of morphological features automatically extracted from H&E slides to predict DLBCL outcomes. The model achieved a concordance index of 0.791 and an AUC of 0.812 for predicting 3-year overall survival [10]. Table 1 shows the most significant work in the field of cell segmentation of H&E-stained histological images as well as in the field of DLBCL detection.

Automated histological image segmentation has advanced considerably thanks to deep learning architectures such as U-Net, DeepCell, and CellProfiler, enabling accurate delineation of cellular contours and morphometric characteristics [12, 16, 17]. However, the application of segmentation methods to H&E images in DLBCL remains quite limited. Naji and colleagues introduced HoLy-Net, based on HoVer-Net [4], for DLBCL image segmentation, achieving an F1-score of 0.899 compared to 0.849 for Mask R-CNN in binary classification of nuclei as "tumor" / "non-tumor" [13].

A critical gap remains the near-total absence of validated computer vision systems for identifying and quantifying TAMs in H&E-stained sections. This is largely because macrophages lack distinct morphological features on H&E staining that would allow for reliable differentiation from histiocytes, endothelial cells, or reactive lymphoid elements [9, 20]. As a result, the vast majority of existing AI solutions for TAM analysis still depend on prior IHC staining, thereby reintroducing the original limitations of that method [5].

There are also several significant technical limitations in current approaches. HoLy-Net is not publicly available, which hinders specific identification of TAMs within the "non-tumor" category in DLBCL. Moreover, there is considerable variability in image quality due to differences in tissue preparation and staining protocols. A major challenge remains the lack of publicly available, well-annotated datasets of DLBCL with H&E staining. Pretrained models based on natural image datasets such as ImageNet perform suboptimally on DLBCL images due to the unique structure of lymphoid tissue.

The shortage of high-quality annotated data has driven the development of SSL methods, which can extract informative domain-specific representations for medical imaging tasks [2, 3]. For instance, Ciga et al. demonstrated that using SSL with the contrastive SimCLR approach on histopathological data provides an absolute increase in classification accuracy by an average of 10.3 percentage points, and segmentation by 6-8 percentage points compared to models pre-trained on ImageNet for ResNet-18/34/50 architectures [3]. Similar results were obtained in a study by Wang et al. where self-supervised methods (for example, DINO based on CTRansPath) on the NCT-CRC-HE dataset demonstrated an increase in accuracy in classification from 87 % (ImageNet) to 95 % (SSL), that is, an increase of 7.97 percentage points (and up to 11-15 percentage points with limited amounts of training data) [19], and Koohbanani et al. demonstrated substantial improvements in tumor region segmentation, outperforming traditional transfer learning approaches and ImageNet-pretrained models [6].

In this context, the development of a deep learning model for automatic identification, segmentation, and quantification of TAMs on standard H&E-stained sections represents a promising direction that addresses current technological limitations.

3 Methods

3.1 Dataset and Annotation

The study utilized 23 WSI microphotographs of DLBCL stained with hematoxylin and eosin (H&E), provided by the Department of Pathology, School of Medicine, Tokai University, Japan. Trained specialists manually annotated 856 macrophages under expert supervision. Additional datasets included LyNSeC (40 DLBCL images) and Immunocto (large-scale immune cell database) for models pretraining. Binary masks were generated using OpenCV, with each labeled macrophage validated and counted. The annotation protocol ensured consistency between experts, with documented uniform markup rules for ambiguous cases. Binary masks were generated using OpenCV, with each labeled macrophage validated and counted. The annotation protocol ensured consistency between experts, with documented uniform markup rules for ambiguous cases.

3.2 Image Patch Segmentation

To build the training dataset, the following strategy was implemented. Microphotographs were divided into non-overlapping patches of 256×256 pixels. Each labeled macrophage was cen-

tered within the patch using geometric transformations (translation and rotation) to prevent the edges of the macrophages from being cut off. This was done to prevent the model from learning on half of a macrophage as the target. To generate background patches, 30 random patches per original image were extracted from macrophage-free regions, ensuring no macrophage presence. The final dataset consisted of 859 macrophage-containing patches and 690 background patches.

3.3 Data Augmentation

For each macrophage-containing patch, 10 additional augmented images were generated using a transformation pipeline implemented with the Albumentations library. A horizontal flip was applied with a 50% probability, and similarly, a vertical flip was applied with a 50% probability. This increased data variability and ensured the model's invariance to object orientation. Color distortions were applied with a 50% probability and included random adjustments to brightness within the range (0.01 to 0.3), contrast (0.01 to 0.3), saturation (0.01 to 0.4), and hue (0.01 to 0.1). These transformations improved the model's robustness to lighting conditions and color variations. Gaussian blur with a fixed kernel size of 3×3 was also applied with a 50% probability to simulate defocus and motion blur effects, enhancing model resilience to image noise and degradation. All transformations were applied stochastically, ensuring a diverse augmented dataset while preserving the semantic integrity of the original images.

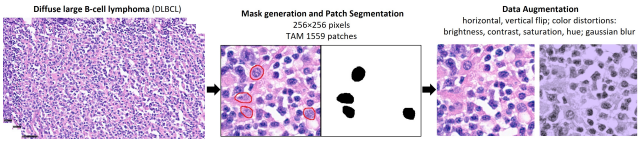

Figure 2. Data preprocessing

3.4 YOLO Training

Training using the prepared training dataset of 18 images, split into patches using the method described above, and similarly 5 images for validation, the YOLOv11 (versions -n, -m). As part of the experiment, a special data set was prepared for one of the training cycles, where the patches were 512x512 pixels. To train the YOLOv11 models, we used the SGD optimizer with an initial learning rate of 0.01, a momentum of 0.937, and regularization weight decay = 0.0005. To control the learning rate change, we used the cosine lr scheduler with a minimum rate of lrf = 0.01 and a warmup phase of 3 epochs. Training was conducted for 60, 100, and 300 epochs; the results are shown in Fig. 1. The evaluated metrics include Precision, Recall, mAP@0.5, and mAP@0.5:0.95.

3.5 Supervised Baseline Training

Supervised Baseline Training: We tested two different approaches of supervised training with models without domain specific pretraining The U-Net model was trained with simple semantic segmentation tasks with patches of TAMs, background and corresponding masks. We used the implementation of U-Net in segmentation models pytorch library with EfficientNet Lite backbone (about 3M parameters) initialized with ImageNet pretrained weights. We trained it for 8 epochs with AdamW optimizer and OneCycleLR scheduler (max_lr: 0.0025, div_factor=25). Experiments with bigger backbones and longer training gained no additional quality. Tversky loss was used with FN penalty 4 times higher than FP penalty due to possible unlabeled TAMs in the images (simple DICE loss showed worse results). We also tested the YOLOv8n-seg model as an example of an instance segmentation approach. We trained it with default parameters except for 32 batch size and 50 epochs. Longer training and bigger models showed equal or worse quality. For segmentation quality assessment we used 5-fold cross validation with splitting by the whole pictures to prevent data leakage caused by intersecting patches.

3.6 Model Architecture and Training

Self-Supervised Learning. The backbone architecture was based on ResNet-18, employing contrastive learning with the NT-Xent loss and LoRA for parameter-efficient fine-tuning. This combination reduces the number of trainable parameters while maintaining model performance.

Self-Supervised Pretraining. Training the feature encoder on the combined dataset without labels. Learning domain-specific representations tailored to DLBCL histological images.

Supervised Fine-Tuning. Training a TAM classifier (the model head) for binary patch classification. Using labeled data to finalize model tuning.

3.7 Self-Supervised Representation Learning (SimCLR + LoRA)

Backbone architecture. A ResNet-18 encoder initialised with standard ImageNet weights serves as the feature extractor. All convolutional layers receive rank-reduction adapters via LoRA (r=8, $\alpha = 16$, dropout=0.1) to enable parameter-efficient fine-tuning.

Projection head and loss. Encoder outputs (512-D) are flattened and passed to a two-layer MLP ($512 \to 512 \to 128$) with BatchNorm and ReLU. Contrastive optimisation uses the *NT-Xent* loss with temperature $\tau = 0.1$.

Data pipeline. Tiles are deterministically split (90% train, 10% val, seed 42). We employ the standard SimCLR augmentation family: RandomResizedCrop(224), horizontal flip, colour jitter (0.8), grayscale ($p = 0.2$), GaussianBlur($\sigma \in [0.1, 2.0]$) and ImageNet normalisation.

Optimisation. Training proceeds for 100 epochs with batch size 4 (limited by GPU memory), Adam (lr=3×10^{-4}, $\beta_{1,2} = (0.9, 0.999)$). A k-NN ($k = 5$) probe on frozen features is executed every 5 epochs.

Evaluation results. We report Top-1 accuracy of a k-NN classifier ($k = 5$) on the validation set after pre-training:

- Random initialization: **0.3122**
- ImageNet initialization: **0.5079**
- SimCLR + LoRA (ours): **0.6878**

3.8 Qualitative Retrieval Comparison

Figure 3 shows, for a single query tile with true label `0_I3`, the nearest-neighbor retrieved by each feature extractor and its predicted label:

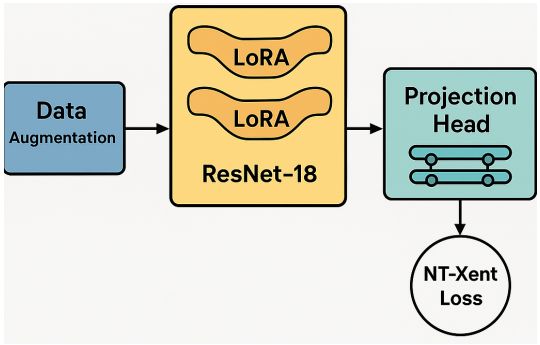

Figure 3. SimCLR+LoRA pipeline: each tile is augmented twice, encoded by ResNet-18 with LoRA adapters, projected to 128D, and trained via NT-Xent loss.

3.9 Nearest-Neighbour Comparison

Figure 4 visualizes, for a single query tiles, the nearest-neighbor retrieved under three feature spaces in one horizontal row.

3.10 SAM ViT-B Fine-Tuning for Binary Segmentation

Base model We fine-tune the **Segment Anything Model (SAM) ViT-B/16**[1] checkpoint `sam_vit_b_01ec64.pth`. All backbone weights are frozen; only `q_proj` and `v_proj` layers receive LoRA adapters (r=16, α = 16, dropout 0.1).

Training hyper-parameters Each fold trains for 10 epochs with batch 4, AdamW (lr = 1×10^{-4}, weight decay 10^{-2}). Loss: `BCEWithLogits`. Best checkpoints are selected by mean IoU on the validation set.

Evaluation metrics Model performance will be evaluated using standard semantic segmentation metrics, such as accuracy and Intersection over Union (IoU), to measure the precision of TAM identification and segmentation boundaries. The k-NN Top-1 accuracy will assess the quality of learned representations during self-supervised pretraining, while DICE coefficient, recall, and precision will evaluate segmentation accuracy. Additional metrics include sensitivity, specificity, and Area Under the Curve (AUC) for binary classification performance. Pixel-wise Precision and Recall – to separately evaluate the ability to detect macrophages (true positives) versus over-segmentation or missing detections.

4 Results

4.1 Supervised baseline

U-Net and YOLOv8 showed quite similar results, metrics are shown in the table below. But as we can see from the picture N due to the instance segmentation task YOLO much better divides TAMs into the different objects, which is more useful for practical usage. Overall even without domain specific pretraining using general domain models reasonably good quality can be achieved.

Table 2
Best results of evaluation of tested models

Model	Precision	Recall	mAP@0.5	mAP@0.5:0.95
yolo11n-seg	0.60121	0.57419	0.61686	0.34585
yolo11m-seg	0.58157	0.54839	0.57328	0.31301
yolo11m-seg512	0.612	0.50883	0.54411	0.27307

4.2 YOLO comparing

Among the evaluated YOLOv11 models (Tab. 2), the yolo11n-seg configuration achieved the best overall performance, with the highest values of Precision — 0.60121, Recall — 0.57419, and mAP@0.5 — 0.61686, as well as the highest mAP@0.5:0.95 — 0.34585. The yolo11m-seg variant trained on 512×512 patches (yolo11m-seg512) demonstrated the highest Precision — 0.612 among all models, but with a trade-off in Recall and mAP values, suggesting a more conservative detection strategy. Other configurations of yolo11m-seg and yolo11n-seg showed moderately consistent results, with some repeated entries indicating re-evaluation under the same settings. Overall, yolo11n-seg exhibited better balance between detection accuracy and generalization compared to the heavier yolo11m-seg models.

Table 3
Summary table with the results of the tested models

Model	DICE	Precision	Recall
U-Net	0.509	0.533	0.507
YOLOv8	-	0.516	0.501
ssl + head	0.516	0.741	0.450

4.3 Results of the tested models

The results of the table show a comparison of the three models using DICE, Precision, and Recall metrics. The U-Net model showed balanced but moderate values: DICE — 0.509, Precision — 0.533 and Recall — 0.507. YOLOv8 does not have DICE values, but showed Precision — 0.516 and Recall — 0.501, which is comparable to U-Net. The ssl + head model stands out most noticeably, which reached the highest Precision value — 0.741, but at the same time showed the lowest Recall — 0.450, which may indicate high accuracy with a reduced level of completeness. According to the DICE metric, it slightly surpassed U-Net, gaining — 0.516.

4.4 Overall survival and progression-free survival

In a cohort of 29 patients provided by the Department of Pathology, School of Medicine, Tokai University, Japan, CD163 levels were analyzed both as continuous percentages and as a binary variable based on an optimal cut-off — 19.68. As a continuous variable, CD163 was not significantly associated with overall survival (OS: HR = 1.02, p = 0.302) or progression-free survival (PFS: HR = 1.02, p = 0.237). When dichotomized, lower CD163 levels were associated with a trend toward better survival outcomes (OS: HR = 0.41, PFS: HR = 0.35), though these results did not reach statistical significance. The limited sample size likely reduced the statistical power, highlighting the need for validation in larger cohorts.

[1] 12 transformer blocks, 768 hidden units, 12 heads, patch size 16 × 16, pretrained on 11M images with 1.1B masks.

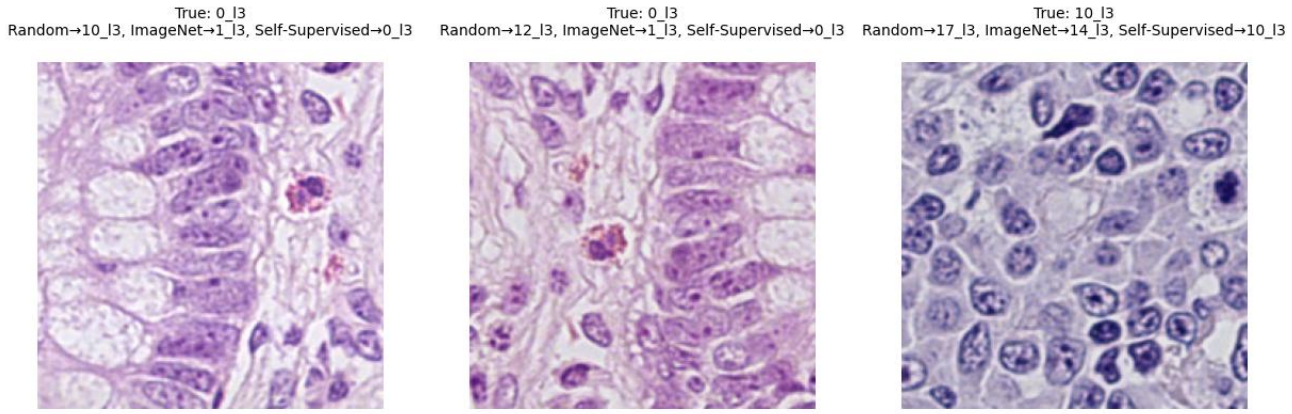

Figure 4. Nearest-neighbor retrieval for query tile with true label 0_I3.

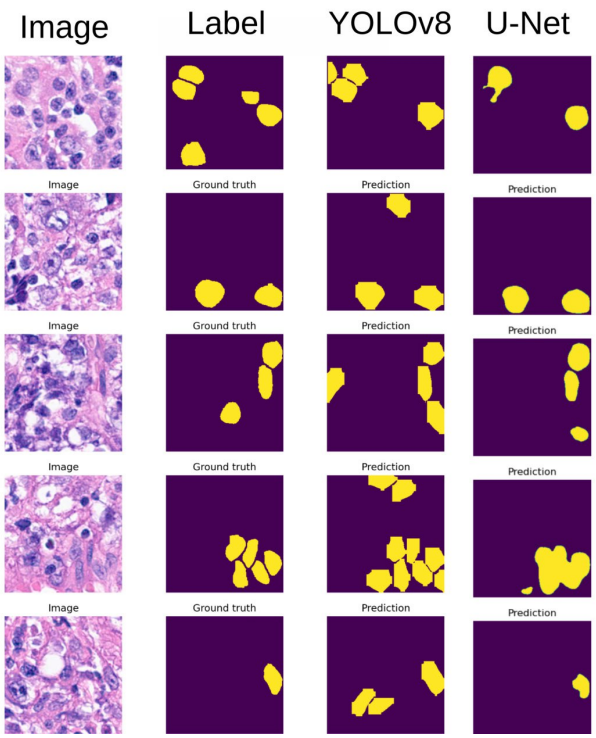

Figure 5. Baseline segmentation results. Ground truth (center) and predicted (right) TAMs are depicted in yellow.

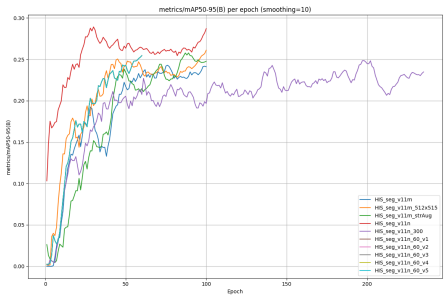

Figure 6. Comparison of the mAP@0.5:0.95 metric for the tested models, when training on 60-300 epochs

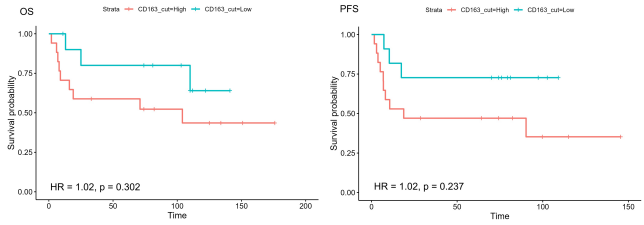

Figure 7. Overall survival and progression-free survival

5 Conclusions

The present study represents the first validated approach for the automated detection of tumor-associated macrophages in diffuse large B-cell lymphoma standard slices stained with hematoxylin and eosin using self-learning algorithms. The developed methodology, based on a combination of SimCLR pre-learning with LoRA adaptation, demonstrates a better quality of feature extraction compared to traditional transfer learning approaches. Despite the fact that the analysis of clinical correlations has revealed promising trends, large-scale validation studies are required to establish the prognostic significance. Nevertheless, the results achieved open up opportunities for reducing diagnostic costs and standardizing the quantification of TAM in routine histopathological practice.

References

[1] N. M. Anderson and M. C. Simon. "The tumor microenvironment". In: *Current biology: CB* 30.16 (2020), R921–R925. DOI: 10.1016/j.cub.2020.06.081.

[2] S. Azizi et al. "Big Self-Supervised Models Advance Medical Image Classification". In: *Proceedings of the IEEE/CVF International Conference on Computer Vision (ICCV)*. 2021, pp. 3478–3488. DOI: 10.1109/ICCV48922.2021.00348.

[3] O. Ciga, T. Xu, and A. L. Martel. "Self-supervised contrastive learning for digital histopathology". In: *Machine Learning with Applications* 7 (2022), p. 100198. DOI: 10.1016/j.mlwa.2021.100198.

[4] S. Graham et al. "HoVer-net: Simultaneous segmentation and classification of nuclei in multi-tissue histology images". In: *Med. Image Anal.* 58 (2019), p. 101563. DOI: 10.1016/j.media.2019.101563.

[5] Y. B. Hagos et al. "ConCORDe-Net: Cell Count Regularized Convolutional Neural Network for Cell Detection in Multiplex Immunohistochemistry Images". In: *Medical Image Computing and Computer Assisted Intervention – MIC-*

CAI 2019. Vol. 11764. Lecture Notes in Computer Science. 2019, pp. 674–682. DOI: 10.1007/978-3-030-32239-7_74.

[6] N. A. Koohbanani et al. "Self-Path: Self-supervision for classification of pathology images with limited annotations". In: *IEEE Transactions on Medical Imaging* 40.10 (2021), pp. 2845–2856. DOI: 10.1109/TMI.2021.3056020.

[7] D. Li et al. "A deep learning diagnostic platform for diffuse large B-cell lymphoma with high accuracy across multiple hospitals". In: *Nature communications* 11.1 (2020), p. 6004. DOI: 10.1038/s41467-020-19817-3.

[8] P. Li et al. "High Counts of CD68+ and CD163+ Macrophages in Mantle Cell Lymphoma Are Associated With Inferior Prognosis". In: *Frontiers in oncology* 11 (2021), p. 701492. DOI: 10.3389/fonc.2021.701492.

[9] Z. Li et al. "Applications of machine learning in tumor-associated macrophages". In: *Front Immunol* 13 (2022), p. 985863. DOI: 10.3389/fimmu.2022.985863.

[10] Z. Li et al. "Machine learning-based histopathological features of histological slides and clinical characteristics as a novel prognostic indicator in diffuse large B-cell lymphoma". In: *Pathology, research and practice* 272 (2025), p. 156071. DOI: 10.1016/j.prp.2025.156071.

[11] M. Lin et al. "The prognostic value of tumor-associated macrophages detected by immunostaining in diffuse large B cell lymphoma: A meta-analysis". In: *Front. Oncol.* 12 (2023), p. 1094400. DOI: 10.3389/fonc.2022.1094400.

[12] P. Manju et al. "A novel approach for nuclei segmentation using U-Net". In: *2023 International Conference on Networking and Communications (ICNWC)*. 2023, pp. 1–6.

[13] H. Naji et al. "HoLy-Net: Segmentation of histological images of diffuse large B-cell lymphoma". In: *Computers in biology and medicine* 170 (2024), p. 107978. DOI: 10.1016/j.compbiomed.2024.107978.

[14] S. Pacis et al. "Epidemiology and Real-World Treatment of Incident Diffuse Large B-cell Lymphoma (DLBCL): A German Claims Data Analysis". In: *Oncology and therapy* 12.2 (2024), pp. 293–309. DOI: 10.1007/s40487-024-00265-8.

[15] E. Silkenstedt et al. "B-cell non-Hodgkin lymphomas". In: *Lancet* 403 (2024), pp. 1791–1807. DOI: 10.1016/S0140-6736(24)00264-3.

[16] D. R. Stirling, A. E. Carpenter, and B. A. Cimini. "Cellprofiler analyst 3.0: accessible data exploration and machine learning for image analysis". In: *Bioinformatics* 37.22 (2021), pp. 3992–3994. DOI: 10.1093/bioinformatics/btab634.

[17] D. A. Van Valen et al. "Deep learning automates the quantitative analysis of individual cells in live-cell imaging experiments". In: *PLoS Comput Biol* 12.11 (2016), e1005177. DOI: 10.1371/journal.pcbi.1005177.

[18] J. Vaughan, T. Wiggill, Z. Mia, et al. "Tumour-associated macrophages in diffuse large B-cell lymphoma: the prognostic and therapeutic impact in a South African centre with high HIV seroprevalence". In: *Immunol Res* 72 (2024), pp. 1393–1403. DOI: 10.1007/s12026-024-09537-x.

[19] X. Wang et al. "TransPath: Transformer-Based Self-supervised Learning for Histopathological Image Classification". In: *Medical Image Computing and Computer Assisted Intervention – MICCAI 2021*. Vol. 12908. Lecture Notes in Computer Science. 2021, pp. 186–195. DOI: 10.1007/978-3-030-87237-3_18.

[20] T. Xie, A. Huang, H. Yan, et al. "Artificial intelligence: illuminating the depths of the tumor microenvironment". In: *J Transl Med* 22 (2024), p. 799. DOI: 10.1186/s12967-024-05609-6.

[21] X. Xu et al. "The prognostic value of tumour-associated macrophages in non-hodgkin's lymphoma: A systematic review and meta-analysis". In: *Scand J Immunol* 91.1 (2020), e12814. DOI: 10.1111/sji.12814.